# Rotationally inelastic collisions of $H_2^+$ ions with He buffer gas: Computing cross sections and rates

Mario Hernández Vera, F. A. Gianturco, R. Wester, H. da SilvaJr., O. Dulieu, and S. Schiller

Citation: The Journal of Chemical Physics **146**, 124310 (2017); doi: 10.1063/1.4978475
View online: http://dx.doi.org/10.1063/1.4978475
View Table of Contents: http://aip.scitation.org/toc/jcp/146/12
Published by the American Institute of Physics

doi: 10.1063/1.4978475



# Rotationally inelastic collisions of $H_2^+$ ions with He buffer gas: Computing cross sections and rates

Mario Hernández Vera,[1] F. A. Gianturco,[1,a)] R. Wester,[1] H. da Silva, Jr.,[2] O. Dulieu,[2] and S. Schiller[3]

[1]*Institut für Ionenphysik und Angewandte Physik, Universität Innsbruck, Technikerstr. 25/3, A-6020 Innsbruck, Austria*

[2]*Laboratoire Aimé Cotton, CNRS, Université Paris-Sud, ENS Paris-Saclay, Université Paris-Saclay, Orsay, France*

[3]*Institut für Experimentalphysik, Heinrich-Heine-Universität Düsseldorf, Universtätsstr. 1, D-40225 Düsseldorf, Germany*

(Received 7 December 2016; accepted 28 February 2017; published online 27 March 2017)

We present quantum calculations for the inelastic collisions between $H_2^+$ molecules, in rotationally excited internal states, and He atoms. This work is motivated by the possibility of experiments in which the molecular ions are stored and translationally cooled in an ion trap and a He buffer gas is added for deactivation of the internal rotational population, in particular at low (cryogenic) translational temperatures. We carry out an accurate representation of the forces at play from an *ab initio* description of the relevant potential energy surface, with the molecular ion in its ground vibrational state, and obtain the cross sections for state-changing rotationally inelastic collisions by solving the coupled channel quantum scattering equations. The presence of hyperfine and fine structure effects in both ortho- and para-$H_2^+$ molecules is investigated and compared to the results where such a contribution is disregarded. An analysis of possible propensity rules that may predict the relative probabilities of inelastic events involving rotational state-changing is also carried out, together with the corresponding elastic cross sections from several initial rotational states. Temperature-dependent rotationally inelastic rates are then computed and discussed in terms of relative state-changing collisional efficiency under trap conditions. The results provide the essential input data for modeling different aspects of the experimental setups which can finally produce internally cold molecular ions interacting with a buffer gas. *Published by AIP Publishing.* [http://dx.doi.org/10.1063/1.4978475]

## I. INTRODUCTION

The physical problem of collisionally cooling simple molecular ions with an additional atomic gas is of intrinsic interest as a benchmark problem in scattering theory and in the manipulations of molecules at low temperatures. More specifically, $H_2^+$ being the simplest of all molecules, there is an additional, profound motivation for its study coming from fundamental physics.

In this field, increasing the accuracy of the values of fundamental constants and testing whether they are truly constant in time and space[1] are a key endeavor that has been ongoing for nearly a century. Because of the central role played by the constants for the laws of physics and for the science of measurement, it is of fundamental importance to develop independent, as well as more accurate and sensitive, measurements for the same constants, since this allows a strong consistency check and, in the case of discrepancy, possibly the discovery of new effects. One such approach is based on the precision optical spectroscopy of rovibrational transitions in the simplest molecules, i.e., the molecular hydrogen ions (MHIs) $H_2^+$, $D_2^+$, and $HD^+$, confined in an ion trap. Since the preparation of such species in specific initial states is an important issue in trap confinements, the present work shall chiefly analyse the collisional physics that will lead to such a state-selected preparation of ions in traps.

These one-electron MHIs have recently emerged as a family of systems at the intersection of atomic and molecular physics, with enormous potential for ultra-high accuracy in the experiments involving them.[2] This potential is due, on the theoretical side, to the possibility to compute *ab initio* all their properties, in particular the levels of their internal state energies,[3] including hyperfine structure,[4,5] as well as the interaction with external fields.[4,6–8] Since the theoretical predictions depend on the values of certain fundamental constants, a comparison between *ab initio* results and data allows for the determination of these constants.

On the experimental side, MHIs can be robustly confined in an ion trap, where sympathetic cooling by laser-cooled atomic ions permits the reduction of their kinetic energies[9] down to a few mK. The variety of physical methods for internal and external-state manipulation known from the field of atomic manipulation, highly successful in atomic clocks and in quantum information studies, should in principle be applicable to MHIs as well. However, the MHIs offer no strongly bound excited electronic states, so that fast spontaneous electronic emission to their ground state is not available. Furthermore, the

a)Electronic mail: francesco.gianturco@uibk.ac.at.

homonuclear MHIs do not have electric dipole-allowed rovibrational transitions. Hence, the standard methods from atomic physics are not transferable in a simple way. Instead, specifically adapted techniques must be developed. In particular, it is desirable to prepare MHIs in a single quantum state, as the most convenient initial condition for spectroscopy.

Suitable states of interest are those having zero or small rotational angular momentum $N$, in which case the hyperfine structure is simpler and thus simpler spectra result. For example, in a $N = 2$ level of $H_2^+$, there are only two hyperfine states (not counting Zeeman sub-levels), and only one in $N = 0$.[10] Preparation in the vibrational ground state $v = 0$ is also desirable as it cannot be further vibrationally deactivated by collisions. In addition, these states are highly suitable for achieving high spectroscopic accuracy.[2,7]

Here we consider a preparation approach that starts with the MHIs produced by standard electron impact ionization, a procedure resulting in populating a large number of rovibrational levels of the produced ion. This can also occur within an ion trap, so that the MHIs are immediately trapped. A co-trapping with continuously laser-cooled beryllium atomic ions can be implemented in order to reduce the (secular, kinetic) temperature of the MHIs to a level of 10 mK by sympathetic cooling. This preparation of the external degrees of freedom can be followed by interaction with a neutral gas at an appropriately chosen temperature, which would then act as a buffer gas for rotational and vibrational cooling: in particular, cryogenic He buffer gas is a practical option from an experimental point of view. The laser cooling of the atomic ions and the resulting sympathetic cooling on the MHIs may be important to counteract any translational heating effect that the buffer gas may exert on the trapped ions. We are not aware of any experimental result on the translational buffer gas cooling of trapped ions which are lighter than the present gas molecules: for simulations see Ref. 11.

In explicit terms, the goal of He buffer gas cooling is to prepare para-$H_2^+$ (total nuclear spin $I = 0$, even $N$) in the ground rovibrational level ($v = 0$, $N = 0$), which has only a single hyperfine state (consisting of two Zeeman sub-states), or in (0,2) level, which has 2 hyperfine sublevels. Ortho-$H_2^+$ (total nuclear spin $I = 1$, odd $N$) shall be prepared in its lowest rotational level (0,1), which exhibits 5 hyperfine sublevels.

If the rotationally and vibrationally excited $H_2^+$ is cooled by He, especially at very low He densities of the order of $n_{He} \simeq 10^9\ cm^{-3}$, reactive collisions should not be relevant and the vibrational deactivation (i.e., cooling to $v = 0$) will occur with a time constant of several seconds.[12–14] In other words, since the reaction forming $HeH^+ + H$ only opens when the molecular ion $H_2^+$ is highly vibrationally excited, we expect that the density of such species formed during the ionization process will not significantly cause losses of the ion of interest here.

Therefore, one of the important questions is whether this deactivation can also be accompanied by rotational cooling within the vibrational ground state and what is its characteristic relaxation time. In this work we shall address these questions within an accurate computational analysis of the relevant quantum processes.

More specifically, we shall first explore the detail of the anisotropic atom-ion interaction in the simpler initial case of a vibrationally cooled ortho-/para-$H_2^+$, molecular partner with a He atom. Following the analysis of the spatial characteristics of the *ab initio* derivation of the forces at play, we shall generate an orientationally anisotropic potential energy surface (PES) that will be employed to investigate rotational state-changing collisional cross sections (both for internal rotational "heating" and internal "cooling" processes). We will initially treat the molecular partner as a rigid rotor (RR) within the harmonic approximation at its equilibrium geometry, $r_{eq}$, given by $r_{eq} = 1.057$ Å. We shall further show that to include the anharmonic effects on the vibrational ground state, the target will slightly modify the shape and energy behavior of the final, state-changing rates.

We shall additionally show that, from the present computational study, the inclusion of either hyperfine structure effect or fine structure coupling during the inelastic dynamics has negligible consequences in obtaining the averaged inelastic cross sections which are produced without fine structure contributions, thereby markedly simplifying the calculation of the final inelastic rates.

Finally, we evaluate a broad variety of the state-changing rates, over a range of temperatures which are representative of those encountered in cryogenic ion traps, and analyze their overall behaviour in terms of propensity rules involving different transitions and their relative magnitudes as a function of the initial rotational level of the molecular partner.

## II. INTERACTION FORCES AND ANISOTROPIC POTENTIAL

One of the earlier *ab initio* calculations of the interaction potential between $H_2^+$ and He was carried out by Falcetta and Siska.[15] They conducted an extensive, high level *ab initio* study of the ground electronic state of $HeH_2^+$, accounting for the long-range interaction, the short-range anisotropy, and the dependence of the potential on $H_2^+$ bond length $r$. They found an energy minimum for the collision complex of 2728 $cm^{-1}$. The complex had a collinear structure with the distance $R = 1.568$ Å between the He atom and the center-of-mass of $H_2^+$ and a slightly elongated geometry of $H_2^+$ with $r = 1.098$ Å.

Subsequently, more extensive calculations of the same non-reactive PES were carried out by Meuwly and Hudson[16] and later on by Mrugala *et al.*[17] who employed coupled-cluster treatments using very large basis sets (aug-cc-PVQZ) and obtained very similar results. A more extensive comparison of these findings will be carried out elsewhere[18] in relation to our present *ab initio* potential which we shall discuss below.

As a matter of fact, an extensive series of *ab initio* calculations for the reactive three-atom system had been carried out by various groups over the years. An example of that type of work also computed the isotopic variants $HD^+$ and $D_2^+$.[19–21] Additional, and more recent, work has also been directed to investigate one of the reactive channels,[22,23]

$$H_2^+(v) + He \leftrightarrows HeH^+ + H, \tag{1}$$

and the outcomes of this reaction have also been studied along the exothermic path (the right-to-left path of the reaction above) that leads to the formation of $H_2^+$ and thus to the destruction of $HeH^+$ molecules. The study followed the low-temperature environment of the interstellar medium, and the most recent reactive potential energy surface (RPES) of Ramachandran *et al.*[22] has been employed for the computational analysis of the reaction Eq. (1)[12–14] at the expected conditions of the early universe chemical environment.

The PES employed by the above studies, and described in detail by Ramachandran *et al.*,[22] was obtained at a very high level of *ab initio* calculations, using the Multireference-Configuration-Interaction (MRCI) approach that included all single and double excitation from the initial Complete-Active-Space_SCF (CASSCF) space. Since it turns out to be of a very similar level of accuracy as those cited earlier in this section, we decided to follow in our present work this latest calculation to extract the non-reactive potential from that surface, as outlined below.

That analysis[22] provided several choices for the final, full PES and also accurate numerical fittings of their extended production of *ab initio* raw points. They reported in fact what they called the $M = 8$ fitting choice using FCI/cc-pVQZ level for the basis set expansion. It is the latter choice which we have employed in the present work, by accurately generating from the initial interacting potential in interparticle coordinates, $V_{M8}(R_1, R_2, R_3)$ of the $(HeHH)^+$ complex, the corresponding non-reactive potential in Jacobi coordinates, $V_{M8}(r_{eq}|R, \theta)$ for the initial system of $H_2^+ - He$,

$$V_{M8}(R_1, R_2, R_3) \rightarrow V_{M8}(R, \theta|r_{eq}), \tag{2}$$

where the $[R, \theta]$ two dimensional (2D) space represents the distance $R$ from the He atom to the mid-bond in $H_2^+$ and the angle $\theta$ is formed between the distance vector and the molecular axis, kept fixed at the ground vibrational state equilibrium value $r_{eq}$.

After the transformation of Eq. (2), we generate four thousand points on the above 2D grid and further produced the corresponding multipolar coefficients $V_\lambda(R|r_{eq})$,

$$V_{M8}(R, \theta|r_{eq}) = \sum_{\lambda=0}^{\lambda_{max}} V_\lambda(R|r_{eq}) P_\lambda(\cos\theta), \tag{3}$$

where

$$V_\lambda(R|r_{eq}) = \frac{2\lambda + 1}{2} \int_{-\pi}^{\pi} V_{M8}(R, \theta|r_{eq}) P_\lambda(\cos\theta) d\cos\theta. \tag{4}$$

The summation in Eq. (3) was extended up to $\lambda_{max} = 20$ to ensure a representation of the potential surface's anisotropy that would reproduce the points from Eq. (2) within a few $cm^{-1}$. We have also extended the calculations to the larger dimensionality of the 3D PES that includes the vibrational effects in the target, as we shall report more extensively elsewhere.[18]

In order to show a more immediate, pictorial view of the potential energy surface for the present situation, we report in Fig. 1 the overall behaviour of the present interaction $V_{M8}(r_{eq}|R, \theta)$. The data in the figure show strong similarities with the same figures reported by the earlier calculations of Ref. 15 and of Ref. 16 that directly generated the non-reactive interaction. The locations of the minima, the relative

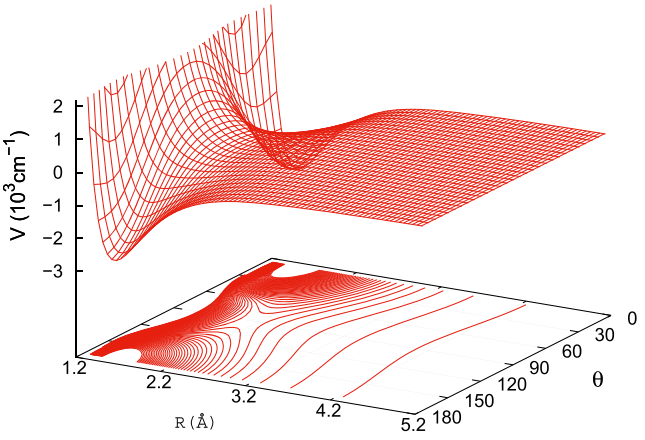


FIG. 1. 3D view and contour plot of the anisotropic potential given by Eq. (2). The potential isolines are separated by 50 $cm^{-1}$. Angles are given in degrees.

well depths, and the comparative strengths of the multipolar coefficients we have found here are very close to those given in the earlier work of Ref. 16. The data confirm the agreement between the present findings from the improved calculations of Ramachandran *et al.*[22] and the earlier *ab initio* results discussed above in this section. As already mentioned, a more detailed comparison of the existing PES will be presented in another publication.[18]

One clearly sees in the figure the steep repulsive region at short distances, which remains so for all orientational approaches, as well as the appearance of the attractive wells symmetrically located along the two collinear approaches for the He partner: the more positively charged, external regions of the H atoms therefore show the most attractive interactions with the polarizable He atom.

That the anisotropy of the interaction is dominated by forces which are symmetric with respect to the homonuclear partner is also shown by the relative strength of the multipolar coefficients from Eq. (3), which are depicted by the curves of Fig. 2.

The most striking result from the shapes of the coefficients reported by Fig. 2 is the fact that the $\lambda = 2$ anisotropic term is the dominant term in the region of the well of the three-atom complex.

The spherical interaction ($\lambda = 0$) extends further out since it corresponds to the term controlled by the spherical (i.e.,

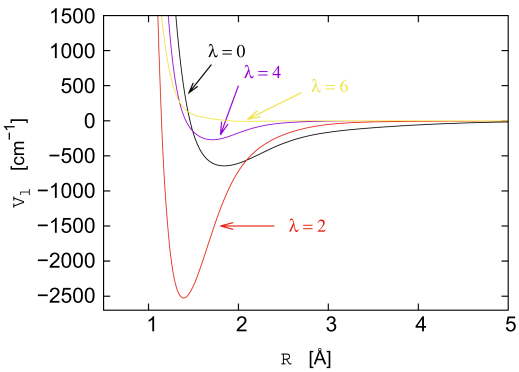


FIG. 2. The computed radial coefficients from the multipolar expansion of the present PES, following Eqs. (2) and (3). Only the first four coefficients of Eq. (3) are shown.

scalar), $\alpha_0$, polarizability of He.[24] We can see that the asymptotic coefficient given by the product $\alpha_0$ with the $H_2^+$ permanent quadrupole moment[15] goes more rapidly to zero but describes also the strongest anisotropic torque, controlled by the $P_2(\cos\theta)$ Legendre polynomial, which is applied during collisions to the molecular rotor by the impinging atom. We shall see below more specific consequences of this feature in our discussion of the relative magnitudes of the inelastic cross sections.

## III. THE QUANTUM TREATMENT OF THE COLLISIONS

### A. The rotational structure of a $^2\Sigma^+$ target molecule

A rotating diatomic molecule with non-zero electron spin and nuclear spin can be approximately described by a Hamiltonian that contains spin-rotation coupling ($H_{sr}$) and hyperfine coupling ($H_{hfs}$) terms in addition to the nuclear rotation term ($H_{rot}$),

$$\begin{aligned} H_{tot} &= H_{rot} + H_{sr} + H_{hfs} \\ &= BN^2 + \gamma \mathbf{S}_e \cdot \mathbf{N} + b\mathbf{I} \cdot \mathbf{S}_e + cI^z S_e^z + f\mathbf{N} \cdot \mathbf{I}. \end{aligned} \tag{5}$$

Here $\mathbf{I}$ is the total nuclear spin, $\mathbf{S}_e$ is the electron spin, and $\mathbf{N}$ is the molecular rotational angular momentum. The largest coefficient is the rotational constant $B$, ($B = 29.65\ \mathrm{cm}^{-1}$, 890 GHz), followed by $b$ (880.162 MHz), by $c$ (128.490 MHz), by $\gamma$ (42.416 MHz), and by $f$ (−0.0417 MHz).[25]

As one can see from the relative values of the coupling terms, the effects of including explicitly the dynamical coupling of spin angular momentum to the rotational angular momentum are likely to influence only marginally the cross section behaviour. We shall report and discuss the details of such coupling effects in Appendix A but we shall carry out the final rate evaluations using only the pseudo-closed shell (i.e., spin-zero) formulation of the scattering problem outlined below.

### B. The coupled channel (CC) equations: A short outline

In the space-fixed (SF) frame of reference, due to the invariance of the potential under rotations of the system, it is convenient to expand the scattering wavefunctions into eigenfunctions $\mathcal{Y}_{jl}^{JM}(\hat{\mathbf{R}}, \hat{\mathbf{r}})$ of the total angular momentum $\mathbf{J} = \mathbf{l} + \mathbf{j}$ to be defined later,

$$\Psi^{JM}(R, r, \Theta) = \frac{1}{R} \sum_{j,l} f_{lj}^J(R) \mathcal{Y}_{jl}^{JM}(\hat{\mathbf{R}}, \hat{\mathbf{r}}), \tag{6}$$

where $\mathbf{l}$ designates the relative orbital angular momentum of the collision partners. The conservation of the parity also constrains the quantum numbers $l$ and $j$, but we do not include the parity index explicitly in the following in order to simplify the notation. The substitution of Eq. (6) in the usual time-independent Schrödinger equation which describes the collisional process leads to the CC equations given by[26]

$$\left( \frac{d^2}{dR^2} + \mathbf{k}^2 - \mathbf{V} - \frac{\mathbf{l}^2}{R^2} \right) \mathbf{f}^J = \mathbf{0} \tag{7}$$

and, as usual, each element of the energy matrix, $k_{ij}^2$, is given as $\delta_{ij} 2\mu(E - \epsilon_i)$, a diagonal matrix for the asymptotic (squared) wavevectors. Here $\mu$ is the reduced mass of the system.

The potential coupling matrix $\mathbf{V} = 2\mu\mathbf{U}$ contains the full interaction potential representation: $\mathbf{U}$, of which the individual terms are typically given by Eqs. (3) and (4). $\mathbf{l}^2$ is the matrix representation of the square of the relative orbital angular momentum $[\mathbf{l}^2]_{ij} = \delta_{ij} l_i(l_i + 1)$. The solution matrix $\mathbf{f}^J$ yields the radial solutions for each selected value of the total angular momentum $J$. In the asymptotic region, the wavefunction solution matrix can be rewritten in order to obtain from it the $\mathbf{K}$ matrix and the scattering matrix, $\mathbf{S}$: $\mathbf{S} = (1 + i\mathbf{K})^{-1} \cdot (1 - i\mathbf{K})$.

For the special case of purely rotational state-changing collisions, the corresponding final, state-to-state, inelastic cross sections are obtained as

$$\sigma_{j \to j'} = \frac{\pi}{(2j+1)k_j^2} \sum_J (2J+1) \sum_{l,l'} |\delta_{lj,l'j'} - S_{lj,l'j'}^J|^2 \tag{8}$$

from the S-matrix elements. Here $j$ denotes the rotational quantum number of the initial rotational state and $j'$ corresponds to the final state. The cross sections describe either a "rotational internal cooling" (RIC) process or a "rotational internal heating" (RIH) process, which for the systems of the present study means $j' < j$ or $j' > j$, respectively. Both situations will be analyzed below for the case of the target molecule $H_2^+$.

### C. The role of the hyperfine structure effects on energy-transfer dynamics

The exact scattering calculations including hyperfine structure terms are obviously able to clarify the role of the electronic and nuclear spins present in $H_2^+$ during the energy-transfer dynamics of the collision. However, given the smallness of such effects, as mentioned before, we will not report the formalism for the quantum dynamics employed to compute the hyperfine-state-resolved cross sections for the title systems. The details of the scattering formulation for the full coupling situation of the open-shell case will be collected in our Appendix B, while in Section IV we will present, as an example of it, the results for the rotational excitation of para-$H_2^+$ system. We shall only report the averaged results for the ortho-$H_2^+$ case, following the simplified scheme that we shall explain below.

### D. The vibration-averaged (VA) potential approach

In this work we are chiefly interested in the rotational (de-)excitation of $H_2^+$ due collisions with He. If we restrict our analysis to the ground vibrational state of $H_2^+$, the simplest approximation is to consider the $H_2^+$ as a rigid rotor (RR) for which the ground-state vibrational wavefunction is further described as a harmonic oscillator (HO). In such a case, then, the convolution of the full interaction over the internal vibrational coordinate yields a delta-function around the $r_{eq}$ value discussed earlier. In other words, the final 2D potential energy surface described by Eqs. (3) and (4) is valid whenever the HO approximation describes well the target vibrational state in question. Thus, the above formulation will be called the HO-RR scheme in the following discussion.

Another possible choice is to explicitly consider the vibrational motion of the molecular target by averaging the PES over the specifically computed ground-state vibrational wave function as given by the potential of the isolated molecular target.

Namely, one can then write

$$V_{00}(R,\theta) = \int_0^\infty \chi^*_{v=0,N=0}(r) V(R,r,\theta) \chi_{v'=0,N'=0}(r) dr, \quad (9)$$

where $\chi_{v,N}$ are the eigenfunctions computed from the Hamiltonian of the isolated vibrating rotor. This scheme shall be called the Vibration-Averaged (VA) computational scheme. We may fix the rotational quantum number $N$ to zero in the above integration because this number does not affect significantly the $\chi_{v=0,N}$ wave functions over the range of rotational energies considered in this work. The $V_{00}(R,\theta)$ function has to be also expanded in terms of Legendre polynomials, as described earlier in Sec. II, in order to implement the new PES in our scattering code in the same way that we did for the calculations within the HO-RR scheme. We will show in Sec. V how the possible deviations of $V_{00}(R,\theta)$ of the VA approach from $V(R,\theta|r = r_{eq})$ of the HO-RR approach, albeit small, can cause changes in the scattering calculations and therefore in the final state-changing rates. The changes would in effect provide a measure of the anharmonic nature of the ground vibrational state of our target molecules and shall be discussed below.

## IV. THE COMPUTED STATE-CHANGING CROSS SECTIONS

In all calculations we have extended the effects of the anisotropic coupling potential out to the external radial region up to around $R_{max} = 50$ Å. The multipolar coefficients of Eq. (3) were included up to $\lambda_{max} = 20$ to represent the full 2D potential of Eq. (2). The integral cross sections were obtained by summing the partial cross sections over a sufficiently large number of values of the total angular momentum $J$ until convergence reached around 1%. The number of $N$ values included in the asymptotic expansion of target states was checked for convergence by having at least two close channels above each energy threshold as part of the full expansion of the coupled-channel wavefunction of Eq. (6), extended and modified by Eq. (B1).

We also carried out numerically converged calculations for the elastic processes, i.e., for the collisions where the molecular rotational quantum numbers did not change. Some examples for the quantities which we have obtained for a very broad range on initial rotational states of the para-target are shown by Fig. 3. The range of collision energies presented runs, for the sake of the example, over a more limited span that which was actually computed for the later studies of the internal cooling in ion traps (to be reported elsewhere).

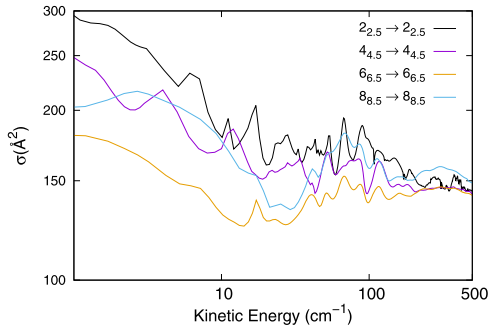


FIG. 3. Kinetic energy dependence of fine-structure elastic cross sections for the para-$H_2^+$. The labeling of the transitions is the following: $N_j \rightarrow N'_{j'}$.

One clearly sees in all cases that the ion-neutral potential of the present systems is yielding very large elastic cross sections: they are all much larger than the molecular "size," as measured by the square of the target bond length. This is also to be expected for scattering processes guided by long-range interactions. Furthermore, we notice also that the larger cross sections occur for elastic collisions with the target in its lower initial rotational states, with the $N = 2$ case producing the largest cross sections, especially at the lower collision energies.

We have also investigated the behaviour of the cross sections for two different sets of state-changing collisional events: (i) the RIC processes, which de-excite the target molecules down to lower rotational internal states, and (ii) the RIH processes, which excite the molecular partners to higher rotational internal states. The results for both sets of processes involving the para-$H_2^+$ molecular ion are reported by the two panels of Fig. 4. Referring to the panels in that figure, we see that the RIC cross sections decrease as $\Delta N$ increases, in accordance with the fact that increasing the energy differences between the involved levels decreases the collisional efficiency of the energy transfer dynamics. Thus, the RIC cross sections at, for example, 200 cm$^{-1}$ of collision energy, drop by a factor of about 4 in the case of para-$H_2^+$ when $\Delta N$ increases from $\Delta N = 2$ to $\Delta N = 8$. Furthermore we see that the strong anisotropy of the Legendre polynomial linked to the $\lambda = 2$ multipolar coefficient of Fig. 2 is mirrored in the dynamics by making the $\Delta N = 2$ transitions to be the largest, since they are dominated by the direct torque caused by that term of the anisotropic potential during collisional encounters.

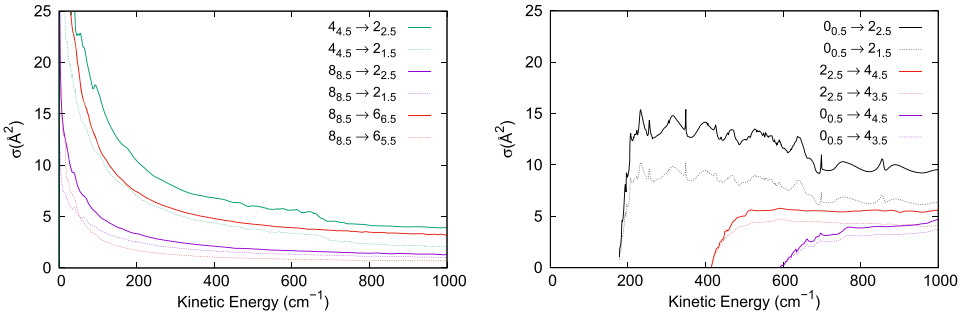


FIG. 4. Kinetic energy dependence of the fine-structure de-excitation and excitation cross sections for the para-$H_2^+$. The transitions are labelled by the main N levels involved and by their fine-structure sublevels as subscripts.

Another clear feature of the cross sections shown in Fig. 4 is the dominance of the $\Delta N = \Delta j$ propensity rule expounded by Eq. (B4): when this happens for a RIC process, the corresponding probability of the process is always larger.

The rotational excitation cross sections, i.e., the RIH collisions, are shown in the right panel of the same Fig. 4. The effect of the decrease of the cross sections as $\Delta N$ increases is here very prominent for the processes involving para-$H_2^+$ which are shown in that panel. The same processes for ortho-$H_2^+$ (not shown in this paper) exhibit smaller cross sections because the corresponding amounts of energy transferred are now larger than for para-$H_2^+$, as shown by the energy level spacings.[27] Additionally, the RIH collisions show in general a weaker presence of resonances than the RIC processes. In any event, the presence of resonances is not expected to play a significant role on the behaviour of the corresponding rates at the temperatures of interest, as we shall further discuss below. In the case of the RIC processes, we also verify here the same propensity rule of $\Delta N = \Delta j$ discussed before.

As mentioned earlier, the coupling between molecular rotations and electronic spin is fairly weak and it therefore affects the rotational state-changing process only indirectly, via the $\mathbf{F} \cdot \mathbf{N}$ recoupling after the collisional partners recede from each other. Thus, we expect that both the fine and hyperfine structure contributions to overall rotational inelasticity should be fairly limited and easily modelled by the averaging procedures that we shall mention below. An example of such options is shown by the calculations in the four panels of Fig. 5, where the computed cross sections are obtained by treating the two target molecules as HO-RR systems without either fine or hyperfine structure effects. In the case of the para-$H_2^+$ system, the present coupling-averaged results are also compared with those more correctly obtained by using the complete angular momentum coupling scheme of the Hund's case mentioned before.

In the top-left panel of Fig. 5 we clearly see that the size and behavior of the rotational de-excitation cross sections computed by including hyperfine structure effects, and summed over all their components, are essentially coincident with the cross sections for the same processes, obtained without including fine structure effects, i.e., considering the collision dynamics of a pseudo-$^1\Sigma$ target molecule.

When we now turn to the RIH processes shown by the bottom left panel of the same figure, we can see again there strong similarities between the results coming from the two angular momenta coupling procedures: they indeed still remain, both in size, energy dependence, and relative behaviors, essentially the same in the two sets of calculations: the difference between the two cross sections in the bottom-left panel is never larger than 10%.

We can conclude from these examples that to obtain the relative strength and energy dependence of the state-changing collisional rates at the typical temperatures in the ion traps, it is quantitatively correct to treat the collisional processes as if occurring with a simpler, pseudo-$^1\Sigma$-type molecular partner. The corresponding results for the ortho-$H_2^+$ are directly shown in the two right panels only for the case of the pseudo-$^1\Sigma$ target molecule. We can notice, like before, that the RIH cross sections for this system are uniformly smaller than those of the corresponding right panel since larger energy transfers are involved here.

In order to extend the simplified coupling procedure to the analysis of the elastic collisions, we further report in the two panel of Fig. 6 some examples for both varieties of molecular targets which we have examined in this work. Because of the strength of the interaction potential, both sets of cross sections exhibit very interesting resonant structures all across the examined energy range, with the features being particularly marked in the low-energy range for both systems.

One interesting feature of these resonances is that they are more prominent in the cross sections where their initial molecular ion is either non-rotating or in low rotational states.

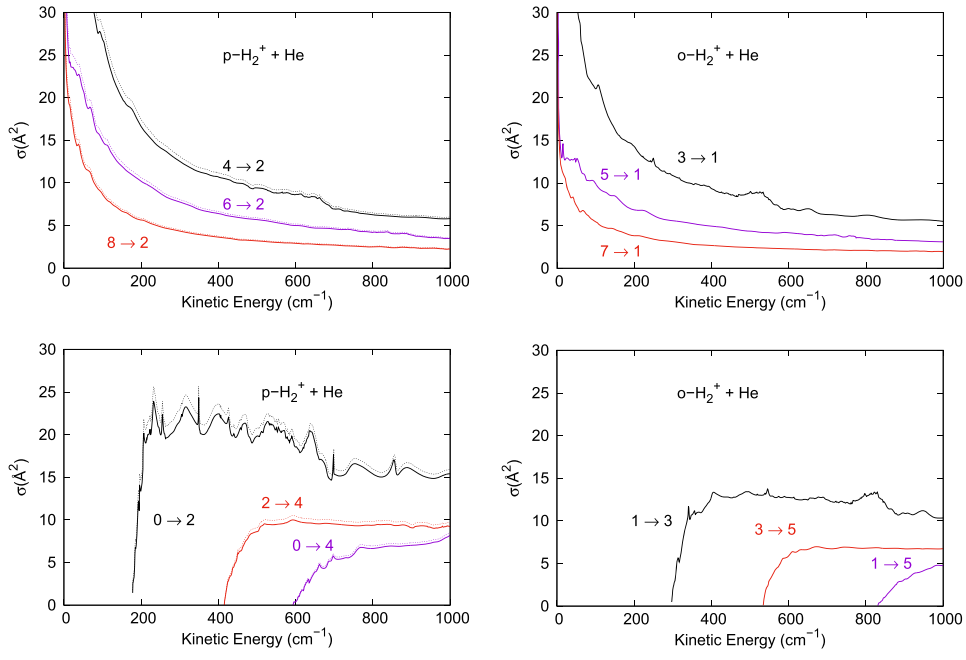


FIG. 5. Left panels: Comparison between pseudo-$^1\Sigma^+$ rotational cross sections (continuous lines) and summed fine-structure cross sections (dashed lines) for para-$H_2^+$. Right panels: All cross sections are calculated among pseudo-$^1\Sigma^+$ rotational state representations for both ortho- and para-MHIs.

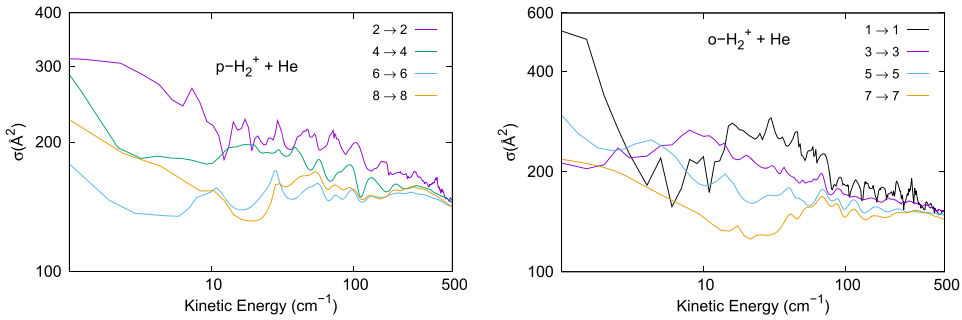


FIG. 6. Kinetic energy dependence of the elastic cross sections for the pseudo-$^1\Sigma$, para-$H_2^+$, and ortho-$H_2^+$. The transitions are labeled by the main N rotational levels involved.

This is due to the fact that, when the molecular partner in the complex is rotationally "hot," the interaction potential supports fewer bound states. Hence, the trapping of He is less efficient, thereby making the resonances more short-lived and less noticeable on the general cross section energy profiles.

To analyze the origin of such resonances is outside the scope of the present study, although we know already that in such ionic interactions the presence of rotational Feshbach resonances and of shape resonances is known to be very likely to occur. We must however note that the large size of the elastic cross sections, in contrast with the sizes of the state-changing processes discussed in the previous figures, is again a clear indication of the strong interaction existing between these colliding partners in the traps.

## V. COMPUTED STATE-CHANGING RATES UNDER ION-TRAP CONDITIONS

To establish a sort of benchmark evaluation of the network of state-changing rates between rotational levels, we have first focused on a range of temperatures from nearly zero to about 100 K in the modelling of the conditions expected in a cryogenically cooled ion trap.

We have carried out the required convolution over a Boltzmann's distribution of relative collision energies $E$ to obtain the rates at a common temperature $T$ of both the ions and the He atoms,

$$k_{j\to j'}(T) = \left(\frac{8}{\pi\mu k_B^3 T^3}\right)^2 \times \int_0^\infty E\sigma_{j\to j'}(E)e^{-E/k_BT}dE, \quad (10)$$

where $k_B$ is the Boltzmann's constant. To simplify the notation, the label $j$ now collectively represents all the relevant quantum numbers already discussed before and used there to classify the collisional processes.

We have evaluated the above rates from a few K up to 100 K employing $\sigma_{j\to j'}$ values up to 4000 cm$^{-1}$. For the integration we started with $E$ values above threshold by about $10^{-3}$ cm$^{-1}$ and employed an unevenly distributed set of energy values which included a total of more than 1000 points. Numerical convergences were checked to be better than $10^{-2}$ in fractional terms. In the calculations for the rates we have employed the cross sections which were computed using, for comparison, the HO-RR but also the more accurate VA scheme described in Sec. III D.

We report in the two panels of Fig. 7 the temperature behaviour of the rates for the collisionally elastic processes: those for the para-system on the left and those for the ortho-system on the right. As expected, and as further confirmed by the comparison with the state-changing rates reported in the additional figures given later, we see that the elastic processes are much larger than the inelastic ones and also have a much more rapid dependence on the temperature: in both panels the rates change by more than one order of magnitude when going from a few kelvin to 100 K. The role of the elastic processes is therefore expected to be important in modeling the overall relaxation under trap conditions, as we shall discuss in a separate paper.

The results given in the two panels of Fig. 8 show the behaviour of the computed rates involving two exemplary situations: (1) the internal cooling rates for transitions where $\Delta N = \Delta j$ (solid line) and (2) the collisional cooling rates for transitions in which $\Delta N \neq \Delta j$ (dashed lines). For simplicity, only the results for the para-$H_2^+$ system are shown there.

The following considerations follow from the inspection of all the results in that figure:

(i) The strength of the state-changing rates are strongly reduced when the $\Delta N = \Delta j$ propensity rule is not satisfied, this reduction being increasingly larger when

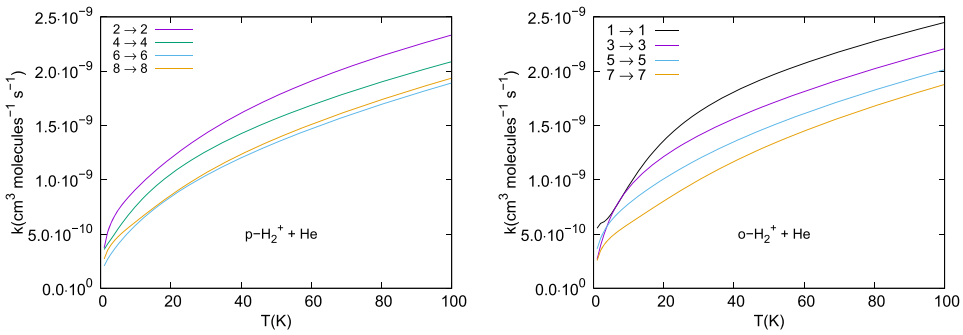


FIG. 7. Temperature dependence of the elastic rate coefficients. The N rotational level indexes are labeling the transitions shown.

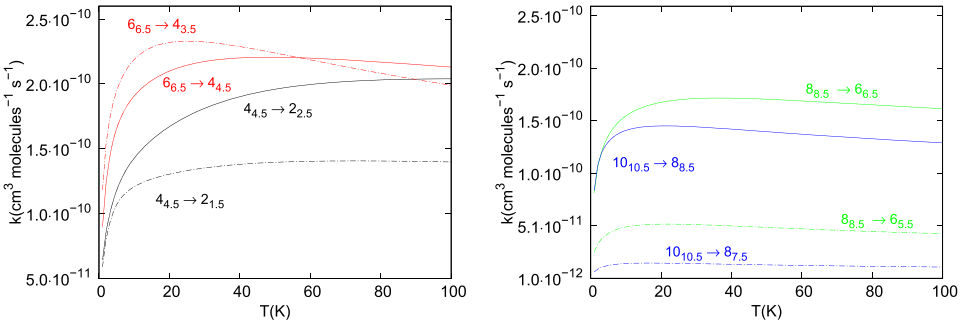


FIG. 8. Temperature dependence of the rate coefficients for $\Delta j = \Delta N$ (continuous lines) and $\Delta j \neq \Delta N$ (dashed lines). Both panels show results for the para-$H_2^+$. The labeling of the transitions is: $N_j \rightarrow N'_{j'}$.

the internal molecular rotational state becomes more excited (larger $N$).

(ii) The above reduction effect is present on all transitions shown in the figure for the para-$H_2^+$ molecular partner. The only exception is the relative behaviour of the $6_{6.5} \rightarrow 4_{4.5}$ vs $6_{5.5} \rightarrow 4_{3.5}$ transitions, involving the states already defined in Secs. III and IV, in the lowest $T$ range from 0 to above 50 K, where the expected reduction is inverted: no numerical reason was found for this effect.

(iii) All the computed rates were found to become smaller when the initial rotational angular momentum $N$ increases. These decreases are not very large and become less important than those associated with the propensity rule effects discussed in (i).

On the whole, however, the state-changing rates around 50 K were found to be of the order of $10^{-10}$ to $10^{-11}$ cm$^3$/s, indicating the cooling/heating processes for the present system to be fairly efficient.

As already discussed earlier, the case $\Delta N = 2$ yields the largest cross sections because the anisotropic interaction between the He atom and the molecular rotor directly associates with the strongest multipolar coefficient with $\lambda = 2$, which means that the corresponding Legendre polynomial efficiently couples initial and final rotational states. It is also interesting to see what happens to these most efficient processes when the target initial $N$ changes. This is shown in Fig. 9 where we also report, for the case of para-$H_2^+$, another comparison between calculations of the rates using the full treatment of the hyperfine structure effects and those obtained using the simpler pseudo-$^1\Sigma$ target molecule dynamics.

(i) The most dramatic difference between the RIC and RIH rates is seen when increasing the initial rotational state of the ions: for the case of para-$H_2^+$ the RIH rates at 80 K change approximately by eight orders of magnitude when the rotational state of the molecular partner increases from $|N = 0\rangle$ to $|N = 8\rangle$ or from $|N = 1\rangle$ state to $|N = 9\rangle$. This increase and also the strong increase of these rates with temperature are both due to a simple threshold effect: the collision energy must exceed the rotational state energy difference. Thus, at low temperatures, it is only the tail of the Boltzmann velocity distribution that contributes to the reaction rate coefficients.

(ii) In the case of the RIC rates (top two panels), their values vary only moderately, albeit non-uniformly, with the increasing initial rotational state quantum number $N$. This is again a truly interaction-related effect, where

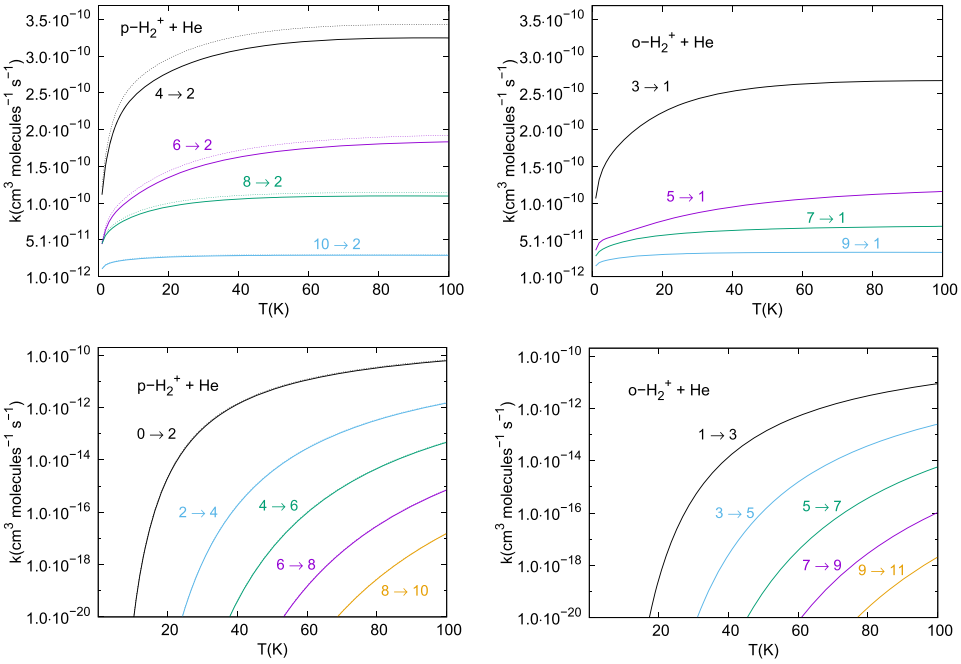


FIG. 9. Left panels: Comparison between the simpler pseudo-$^1\Sigma$ RR rate coefficients (continuous lines) and the summed hyperfine-structure rate coefficients (dashed lines) for para-$H_2^+$. Right panels: Behaviour of the simpler pseudo-$^1\Sigma$ RR rate coefficients for ortho-$H_2^+$. The bottom panels are in a logarithmic scale. The individual curves are labeled by the indexes of the corresponding N rotational levels.

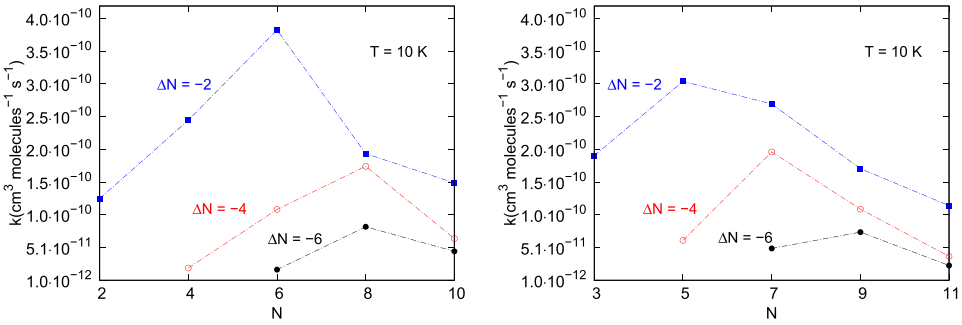


FIG. 10. De-excitation rate coefficients at 10 K for different initial values of $N$ for para-$H_2^+$ – He (left panel) and ortho-$H_2^+$ – He (right panel) collisional systems.

we see that the particular initial-value of $N$ plays a minor role in the RIC processes.

(iii) The plots in Fig. 9 show once more that the results obtained with the simplest approximation, i.e., the VA model (without spin effects included), are very similar to, and at times practically coincident with, the quantum results obtained from the more accurate treatment of angular momenta's couplings. This is an important result which suggests that one can carry out computational simplifications without substantial losses of numerical accuracy in evaluation the state-changing rates.

In Fig. 10 we further examine the dependence of the RIC rate coefficients on the magnitude of the $N$-changing value during the inelastic processes. Thus, we report there the dependence of the rates on the initial $N$ and also on the $\Delta N$ values for a temperature of 10 K, which, from a practical point of view, is similar to the lowest temperature that will occur in an ion trap cooled by a standard closed-cycle cooler.

We clearly see there that the rate coefficients markedly decrease as $\Delta N$ increases. This is a consequence of at least two factors: (1) the angular momentum reorientation factor, $K$, in Eq. (B4) and (2) the energy factor associated with the amount of energy being transferred away from the internal energy content of the partner molecules. The former factor, the change of $K$, correctly reflects into yielding smaller rates (i.e., opacities in Eq. (B4)) as $K$ increases and also $|\Delta N|$ increases. The latter factor, the energy exchange, also reduces the size of the cross sections as $|\Delta N|$ increases.

We also see, however, that the dependence on the initial $\Delta N$ of the molecular partner is not uniform: all the $|\Delta N|$ cases shown in both panels vary rather uniformly with the mutual rotational state of the targets, although no uniform decrease with increasing mutual $\Delta N$ is observed.

We further report in Fig. 11 the RIC rates for $N = 10$ and $N = 11$ as a function of $N'$ and for three different values of relevant temperatures. We see now that the rate coefficients decrease with the increase of $\Delta N$ at all the examined temperatures. This decrease is by nearly two orders of magnitude when $\Delta N = -10$. We can therefore infer from the above findings that the most efficient processes for bringing the rotationally excited initial states of both para-$H_2^+$ and ortho-$H_2^+$ down to their $|N = 0, 1\rangle$ levels would chiefly occur via a multistep chain of processes which come down the population ladder by $|\Delta N| = 2$ jumps.

We report additional results, which further illustrate the behaviour of the present systems during state-changing collisions, in the two panels of Fig. 12. We show there the RIC rates as a function of temperature and for transitions involving $\Delta N = -2$ transitions that start from different $N$ values. We further compare the rates, for both para-$H_2^+$ and ortho-$H_2^+$ systems, for two different numerical schemes that treat the ground vibrational level occupied by the target molecules: the HO approximation of the RR scheme, given by the solid lines, and the VA treatment of the ground vibrational state given by the dashed lines.

There are several observations which can be made by examining the results of Fig. 12:

(i) Over the range of examined temperatures we clearly see that, at least for $N$ up to $N_{max}$ = 10–11, the variations of the rates are all rather modest. The rates on the left panel, in fact, vary at most by a factor of 3 to 4, while those in the right panel vary by even a smaller factor. In other words, for the $\Delta N = -2$, an inelastic process which associates with the most efficient state-changing collisions, the actual initial rotational

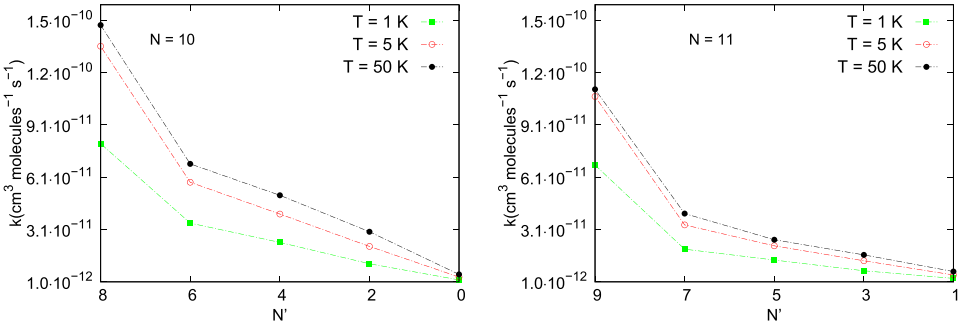


FIG. 11. De-excitation inelastic rate coefficients from $N = 10$ and $N = 11$ at different temperatures for para-$H_2^+$ – He (left panel) and ortho-$H_2^+$ – He (right panel) collisional systems.

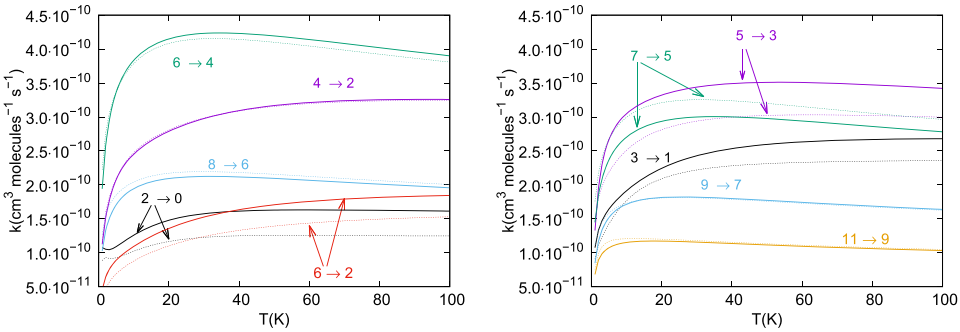


FIG. 12. Comparison between rates coefficients for $\Delta N = -2$ transitions computed with the HO-RR approach (continuous lines) and the VA potential (dashed lines). Left panels: results for the para-$H_2^+$ target molecule. Right panel: for the ortho-$H_2^+$ target. The labeling refers to the initial and final N rotational levels involved in the transitions.

state of the molecular partner plays a rather minor role.

(ii) We also see from the data in the figure that the scaling of the rates as the $|N\rangle$ state changes is not uniform since the increase of the energy gap when going from initial $|N = 2\rangle$ to initial $|N = 10\rangle$ does not cause a uniform reduction of the rates, the same being true also for ortho-$H_2^+$.

If we now observe the different rates computed either within the HO-RR scheme discussed in Sec. III D (continuous lines) or by using the VA scheme (dashed lines), then the following comments can be made:

(i) The consequence of including anharmonic effects when building the rotation-coupling potential, i.e., the VA scheme described in Sec. III D, is mainly that of making the corresponding rates smaller over the whole range of temperatures examined here.

(ii) The size of the changes, however, is not the same for all RIC transitions. For both molecular partners, in fact, we see that the largest changes occur when the lowest initial $N$ states are considered, while for cooling processes from the higher $N$ states the changes are fairly small and practically of not much importance.

(iii) It therefore seems, from the present analysis, that the actual inclusion of the correct physical wavefunction to describe the ground vibrational state of the present systems within the rotationally inelastic dynamics does play a noticeable role on the final sizes of the corresponding rates. Thus, in our further study of modeling rotational relaxation during actual trap physical conditions we shall employ for both systems the corresponding VA-computed rates within the pseudo-$^1\Sigma$ treatment of the CC dynamics.

## VI. PRESENT CONCLUSIONS

The results of the present calculations provide the fundamental input for evaluating the efficiency of collisional cooling in the case of rotationally excited states of both para-$H_2^+$ and ortho-$H_2^+$ by a cold gas of He atoms. We have focussed our study on the exit channels associated with the rotation-only internal state-changing collisions, with the molecular ion in its ground vibrational level. We have further tested the numerical consequences of two different computational schemes for producing an interaction potential that includes the presence of the ground vibrational state in each system.

To this end, we have first obtained the full anisotropic 2D and 3D potential energy surfaces using high-level *ab initio* calculations[22] and then cast the latter in the multipolar form indicated by Eqs. (3) and (4). This shows the dominant strength of the coupling potential component associated with the $P_2(\cos\theta)$ Legendre polynomial. This characteristic of the interaction potential is reflected into the dominance of direct $|\Delta N| = 2$ processes in the state-changing dynamics. This feature affects all the cross sections and rates reported in our work.

The target molecule, even in its ground vibrational state, is not exactly a harmonic oscillator. This means, for the present dynamical study, that small anharmonic effects need to be included and indeed modify the size of the final rates associated with pure rotational state-changing processes.

Another important issue of the quantum dynamics for the title system is that regarding the most efficient choice of the total angular momentum representation for the scattering wavefunction during collisions. The correct physical choice turns out to be the one which explicitly includes spin-rotation effects during the dynamical evolution, a property due to the physics stemming from the $^2\Sigma$ electronic state of the molecular ion. However, our calculations show that summing over fine-structure recoupling terms produces very similar summed cross section values and rate coefficients as those obtained by directly treating the target molecule as a simpler rigid rotor in a pseudo-$^1\Sigma$ state. This is an important result which strongly suggests that all numerical modeling for the collisionally inelastic dynamics can be safely, and accurately, carried out by using the simpler angular momentum representation of the pure rigid rotor target interacting with a closed-shell atom in its zero total angular momentum. Given the nature of intermolecular force between diatomic ions and He atoms, we feel that such a reduction of computational efforts could also yield similar results for many other systems.

We have also investigated the validity of simple propensity rules to scale the cross sections (and hence the ensuing rates) within a manifold of different processes among diverse initial and final levels. The tests we have carried out indicate that the propensity rules outlined by Eq. (B4) with respect to angular momentum reorientations during collisions are indeed valid for the present case. Our calculations indicate that such rules tend to favour the $\Delta N = \Delta j$ processes and increase their efficiency when the rotational angular momentum transfer values during inelastic transitions become increasingly smaller and

approach zero: the marked increase in the size of the elastic cross sections is an indicator of the extreme tendency of this effect.

Finally, the changes of the rate magnitudes when changing the initial and/or final $N$ value of the target state indicate that the $|\Delta N| = 2$ RIC and RIH processes are the dominant ones within the manifold of the many transitions involved. This therefore means that any cooling process to the ground rotational level would evolve via a cascade of transitions from the highest initial levels occupied by the molecular ions in the trap.

## ACKNOWLEDGMENTS

This work has been made possible by the COMIQ Marie Curie Initial Training Network FP7-PEOPLE-2013-ITN: COMIQ: Cold Molecular Ions at the Quantum limit funded by the European Commission under Grant Agreement No. 607491. It has supported all the research groups authoring this paper. The Innsbruck group also thanks the Austrian Science Fund FWF, Project No. P27047-N20. The computational results presented have been achieved (in part) using the HPC infrastructure LEO of the University of Innsbruck.

We are also grateful to Dr. C. N. Ramachandran for providing us with the routine that calculates the initial reactive PES.

## APPENDIX A: SPIN-ROTATION AND HYPERFINE COUPLING TERMS

In the Hund's case ($b_{\beta S}$),[27] the electronic spin, $\mathbf{S}_e$, and the total nuclear spin $\mathbf{I}$ couple together to yield a total spin vector $\mathbf{F} = \mathbf{S}_e + \mathbf{I}$. Since in the general case the vector $\mathbf{F}$ is further coupled to the molecular rotation vector $\mathbf{N}$, we additionally have that each hyperfine level is designated by a quantum number $j$ ($\mathbf{j} = \mathbf{F} + \mathbf{N}$) varying between $|N - F|$ and $N + F$. In the present, homonuclear molecule $I$ takes on integer values, including 0. The even values of $I$ (including 0) are called para, while the odd values are called ortho. In the case of $H_2^+$, only the para state has $I = 0$. The symmetrization postulate requires that para-states have rotational angular momenta $N = 0, 2, 4, \ldots$, while ortho-states have odd $N$ values.

In para-$H_2^+$ ($I = 0$), we have the direct coupling only between $\mathbf{N}$ and $\mathbf{S}_e$. This simplification leads to the fine structure levels with $j = N + 1/2$ and to those with $j = N - 1/2$. In this specific case, therefore, we can directly evaluate the expectation value of the spin-rotation interaction,

$$\begin{aligned}\langle H_{sr}\rangle &= \gamma\langle \mathbf{S}_e\cdot\mathbf{N}\rangle = \gamma\times\frac{1}{2}\langle \mathbf{j}^2 - \mathbf{S}_e^2 - \mathbf{N}^2\rangle \\ &= \frac{\gamma}{2}\left(j(j+1) - \frac{3}{4} - N(N+1)\right) \\ &= \begin{cases} \dfrac{\gamma}{2}N, & j = N + \dfrac{1}{2}, \\ -\dfrac{\gamma}{2}(N+1), & j = N - \dfrac{1}{2}, \end{cases}\end{aligned} \tag{A1}$$

it therefore follows that the expressions for the rotational energies are

$$E_{N_{j=N+1/2}} = BN(N+1) + \frac{1}{2}\gamma N, \tag{A2}$$

$$E_{N_{j=N-1/2}} = BN(N+1) - \frac{1}{2}\gamma(N+1). \tag{A3}$$

Since the above coupling sequence is satisfied in our systems, in the $N = 2$ case, for example, we should have shifts of $\gamma$ and $-3\gamma/2$. As a matter of fact, the earlier calculations of Karr *et al.*[11] find the shifts +42.16 MHz for the $j = 3/2$ level and −63.24 MHz for the $j = 1/2$ level, as it is to be expected.

In the different situation of the ortho-$H_2^+$ ($I = 1$) system, we now have two initial sublevels corresponding to $F = 1/2$ and $F = 3/2$. These sublevels are further split into 5 (for $N = 1$) or 6 (for $N \geq 3$) $j$ sublevels due to the spin-rotation interaction. It is actually known[11] that in the ortho variety the spin-spin coupling is one order of magnitude larger than the spin-rotation coupling. One can therefore approximate that, for a given $N$, each of the states $|N, F = 1/2, j, M_j\rangle$ and $|N, F = 3/2, j, M_j\rangle$ can be considered to be degenerate, thereby simplifying the hyperfine structure effects.

We can therefore evaluate the expectation values of the hyperfine interaction by neglecting the terms $I_z S_z$ and $\mathbf{S}_e \cdot \mathbf{N}$, which are found to be smaller when compared to $\mathbf{S}_e \cdot \mathbf{I}$,

$$\begin{aligned}\langle H_{hfs}\rangle &= b\langle \mathbf{S}_e\cdot\mathbf{I}\rangle = b\times\frac{1}{2}\langle \mathbf{F}^2 - \mathbf{S}_e^2 - \mathbf{I}^2\rangle \\ &= \frac{b}{2}(F(F+1) - \frac{3}{4} - 2) \\ &= \begin{cases} \dfrac{b}{2}, & F = \dfrac{3}{2}, \\ -b, & F = \dfrac{1}{2}. \end{cases}\end{aligned} \tag{A4}$$

From the above formulation, the total energies are now given as

$$E_{N_{F=3/2}} = BN(N+1) + \frac{b}{2}, \tag{A5}$$

$$E_{N_{F=1/2}} = BN(N+1) - b, \tag{A6}$$

which is in agreement with what has been found by Karr *et al.*,[11] who, for the state $N = 1$, gave a shift of 461 MHz for the $F = 3/2$ level and −923 MHz for the $F = 1/2$ level. These two levels are further split by the spin-rotation interaction, but this splitting is only 90 MHz and 20 MHz, respectively. It therefore becomes acceptable to neglect such splitting in the following discussion and calculations for the ortho-$H_2^+$ system.

One should also be reminded at this point that the ortho-to-para conversion between molecular states is forbidden during the inelastic collisional processes that we shall consider in this study. The two types of molecular states will thus be treated as entirely independent systems during the scattering calculations.

## APPENDIX B: DYNAMICS WITH FINE-STRUCTURE EFFECTS

The standard space-fixed (SF) formulation of the quantum scattering within the CC formalism outlined earlier deals only with a $^1\Sigma^+$ molecule interacting with a $^1S$ atom.[28] The changes

necessary for the present case of a $^2\Sigma^+$ molecule have been worked out in detail by many authors over the years[29–31] and will not be extensively reviewed again here.

In analogy with the standard CC formalism,[28] one defines a total angular momentum representation by expanding the atom-molecule wavefunction in eigenfunctions of the total angular momentum $J$, thereby producing

$$|(NF)jl;JM\rangle = \sum_{m_j m_l} (jm_j lm_l|JM) \times |NFjm_j\rangle\,|lm_l\rangle\,, \tag{B1}$$

where $|NFjm_j\rangle$ is the molecular wave function and $|lm_l\rangle$ is the basis set for the relative orbital motion of the colliding pair, and $(\ldots.|..)$ is a Clebsch-Gordan coefficient. The above representation may also be given by the following vector coupling scheme:

$$\mathbf{N}+\mathbf{F}=\mathbf{j};\ \mathbf{j}+\mathbf{l}=\mathbf{J}. \tag{B2}$$

The ensuing development of the coupled equations that now modify the CC scheme of Eq. (B1) is carried out in the new total-$J$ representation[29] that produces the scattering matrix elements given as $S^J_{FNjl,FN'j'l'}$. They will be in turn employed to provide the corresponding state-to-state scattering amplitudes between the relevant channels. From the latter quantities we shall then produce the state-to-state partial integral cross sections summed over final and averaged over initial degeneracies, i.e., the $\sigma(NFj \rightarrow N'Fj')$ cross sections already defined in earlier work.[29]

We have introduced the CC formulation outlined above for scattering from $^2\Sigma$ target molecules in our earlier computational code[32] and have therefore generated with it the relevant network of cross sections for the case of p-$H_2^+$. The numerical details of those calculations will also be given later on.

One should also keep in mind that in the Hund's case ($b_{\beta S}$) coupling scheme the total spin and rotational angular momentum are only weakly coupled. In fact, since the internuclear forces are basically electrostatic in origin, there is no direct effect coming from the spin state of the target, so that binary collisions in the trap do not directly influence either the magnitude or the orientation of the spin angular momentum **F**. There is, however, an indirect effect of the collision dynamics on the rotational angular momentum **j** since both **N** and **F** recouple again after the particles recede from each other. One can therefore take advantage of this mechanism to decouple the total spin **F** from the rotational-centrifugal motion by utilizing a total-**J** representation defined by the coupling scheme,

$$\mathbf{N}+\mathbf{l}=\mathcal{J};\ \mathcal{J}+\mathbf{F}=\mathbf{J}. \tag{B3}$$

As a matter of fact, it was already shown by different authors[29] that using the above coupling one can express the S- or T-matrix elements already mentioned before, e.g., the $T^J_{FNjl\rightarrow FN'j'l'}$ matrix elements, in terms of simpler, spin-independent $T^{\mathcal{J}}_{Nl,N'l'}$ matrix elements, and still be able to get information on the hyperfine-structure transitions.

This problem was further considered in detail in the earlier work by Alexander and co-workers, who analyzed the physical effects of such decoupling on the hyperfine structure transitions.[30,31] They derived physically based propensity rules that govern the relative probabilities of collision-induced transitions between hyperfine-structure levels of $^2\Sigma$ molecular targets. Thus, one obtains the following relationship for the cross section of a particular $(FNj \rightarrow FN'j')$ transition as a sum of irreducible tensorial components of order $K$:

$$\sigma_{FNj\rightarrow FN'j'} = \frac{\pi}{k^2}(2j'+1)\sum_K \begin{Bmatrix} N & N' & K \\ j' & j & F \end{Bmatrix}^2 P^K(N',N), \tag{B4}$$

where $\{:::\}$ is a 6j symbol and each term $P^K$ $(N', N)$ contains the transition probability (i.e., opacity) value which are summed together to yield the relevant cross section. The angular momentum transfer index $K$ can be interpreted as a measure of the degree of reorientation of **N**. The latter quantity was already defined in Sec. III as representing the molecular rotational quantum number of the target molecule. It is also useful to remember that the $F = 3/2 \rightarrow F = 1/2$ collision-induced transitions are forbidden during the excitation of the ortho-$H_2^+$ because the total (nuclear+electronic) spin state is not affected by the collision.

Eq. (B4) indicates that the small collision transfers of angular momentum correlate with small nuclear rotational angular momentum reorientation angles. The contribution of each term decreases as $K$ increases, which is in fact a manifestation of the propensity toward the conservation of the orientation of $N$. Furthermore, for $\Delta N = \Delta j$ transitions, the angular momentum coupling described by the 6$j$ symbol in Eq. (B4), preferentially weights collisions that cause a small reorientation of **N**. This is the main reason for the observed propensity rules in favor of $\Delta N = \Delta j$, a feature that was also observed in earlier calculations.[31] We shall therefore show in the present study that the rotational cooling of $H_2^+$ by collisions with He atoms under the trap conditions discussed in our introduction also follows the behaviour surmised by the above propensity rules.


[1] J.-P. Uzan, Living Rev. Relativ. **14**, 2 (2011).
[2] S. Schiller, D. Bakalov, and V. I. Korobov, Phys. Rev. Lett. **113**, 023004 (2014).
[3] V. I. Korobov, L. Hilico, and J.-P. Karr, Phys. Rev. Lett. **112**, 103003 (2014).
[4] D. Bakalov, V. I. Korobov, and S. Schiller, Phys. Rev. Lett. **97**, 243001 (2006).
[5] J.-P. Karr, V. I. Korobov, and L. Hilico, Phys. Rev. A **77**, 062507 (2008).
[6] D. Bakalov and S. Schiller, Appl. Phys. B **114**, 213 (2014).
[7] J.-Ph. Karr, J. Mol. Spectrosc. **300**, 37 (2014).
[8] S. Schiller, D. Bakalov, A. K. Bekbaev, and V. I. Korobov, Phys. Rev. A **89**, 052521 (2014).
[9] P. Blythe, B. Roth, U. Fröhlich, H. Wenz, and S. Schiller, Phys. Rev. Lett. **95**, 183002 (2005).
[10] J.-P. Karr, F. Bielsa, A. Douillet, J. Pedregosa Gutierrez, V. I. Korobov, and L. Hilico, Phys. Rev. A **77**, 063410 (2008).
[11] R. G. DeVoe, Phys. Rev. Lett. **102**, 063001 (2009).
[12] S. Bovino, M. Tacconi, F. A. Gianturco, and D. Galli, Astron. Astrophys. **529**, A140 (2011).
[13] S. Bovino, M. Tacconi, and F. A. Gianturco, J. Phys. Chem. A **115**, 8197 (2011).
[14] S. Bovino, F. A. Gianturco, and M. Tacconi, Chem. Phys. Lett. **554**, 47 (2012).
[15] M. F. Falcetta and P. E. Siska, Mol. Phys. **97**, 117 (1999).
[16] M. Meuwly and J. M. Hutson, J. Chem. Phys. **110**, 3418 (1999).
[17] F. Mrugała, V. Špirko, and W. P. Kraemer, J. Chem. Phys. **118**, 10547 (2003).
[18] I. Iskandarov, M. Hernández Vera, H. Da Silva, Jr., F. A. Gianturco, R. Wester, and O. Dulieu, "Shape and strength of dynamical couplings

between vibrational levels of the $H_{+2}$, $HD_{+}$, and $D_{+2}$ molecular ions in collision with HE as a buffer gas" (unpublished).
[19]P. Palmieri, C. Puzzarini, V. Aquilanti, G. Capecchi, S. Cavalli, D. D. Fazio, A. Aquilar, X. Giménez, and J. M. Lucas, Mol. Phys. **98**, 1835 (2000).
[20]A. K. Tiwari and N. Sathyamurthy, J. Phys. Chem. A **110**, 11200 (2006).
[21]B. Lepetit and J. M. Launay, J. Chem. Phys. **95**, 5159 (1991).
[22]C. N. Ramachandran, D. De Fazio, S. Cavalli, F. Tarantelli, and V. Aquilanti, Chem. Phys. Lett. **469**, 26 (2009).
[23]D. De Fazio, M. de Castro-Vitores, A. Aguado, V. Aquilanti, and S. Cavalli, J. Chem. Phys. **137**, 244306 (2012).
[24]D. M. Bishop and J. Pipin, Chem. Phys. Lett. **236**, 15 (1995).
[25]V. I. Korobov, L. Hilico, and J.-P. Karr, Phys. Rev. A **74**, 040502 (2006).
[26]R. Martinazzo, E. Bodo, and F. A. Gianturco, Comput. Phys. Commun. **151**, 187 (2003).
[27]J. M. Brown and A. Carrington, *Rotational Spectroscopy of Diatomic Molecules* (Cambridge University Press, 2003).
[28]A. M. Arthurs and A. Dalgarno, Proc. R. Soc. A **256**, 540 (1960).
[29]G. C. Corey and F. R. McCourt, J. Phys. Chem. **87**, 2723 (1983).
[30]M. H. Alexander, J. Chem. Phys. **76**, 3637 (1982).
[31]M. H. Alexander, J. E. Smedley, and G. C. Corey, J. Chem. Phys. **84**, 3049 (1986).
[32]D. López-Durán, E. Bodo, and F. A. Gianturco, Comput. Phys. Commun. **179**, 821 (2008).